Thermal Science and Engineering Progress 42 (2023) 101906

Contents lists available at ScienceDirect

Thermal Science and Engineering Progress

journal homepage: www.sciencedirect.com/journal/thermal-science-and-engineering-progress

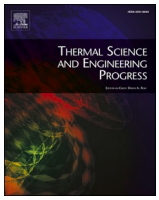

Thermal stability investigations of different aerogel insulation materials at elevated temperature

Zsolt Kovács [a], Attila Csík [b], Ákos Lakatos [c,*]

[a] University of Debrecen, Doctoral School of Earth Sciences, Egyetem Tér 1, Debrecen H-4032, Hungary
[b] Institute for Nuclear Research, Bem tér 18/c, Debrecen H-4026, Hungary
[c] University of Debrecen, Faculty of Engineering, Department of Building Services and Building Engineering, Ótemető Str 2-4, Debrecen 4028, Hungary

ARTICLE INFO

Keywords:
Super thermal insulations
Aerogels
XRD
DSC
Thermal conductivity
Specific heat capacity
Microscopy

ABSTRACT

Super thermal insulation materials with low thermal conductivities, such as aerogels and vacuum insulation panels, are increasingly pushing conventional thermal insulations out of the market. Super insulation materials such as aerogels can be used easily on both vehicles and buildings. Nowadays, their usage by pipes transporting hot medium is also widespread. In these environments where elevated temperatures (100–250 °C) are applied, it is a basic requirement that they should keep their excellent thermal insulating capability. In this study, a comprehensive examination performed on two new silica-aerogel type insulations is presented. We investigated the change in the thermal performance of different types of aerogel insulations (Slentex and Pyrogel) after thermal annealing, ageing them at 150 and 250 °C temperatures for 1 day. After these thermal treatments, their thermal parameters such as thermal conductivities and specific heat capacities were measured. We revealed that both the thermal conductivity and the specific heat capacity for the Pyrogel changed considerably after annealing, while for Slentex the thermal conductivity remained constant and the specific heat capacity changed. To understand these changes we executed calorimetry tests and microscopic inspections with different methods. These experiments were completed with X-ray diffractometry to analyze the possible structural changes in the samples. From an application point of view, we consider the importance of these results, since they predict the lifetime of the used insulating material during their industrial use.

1. Introduction

The high energy use and the emission of greenhouse gases have a negative effect on the climate. Most of the energy used comes from buildings and another huge part of the energy consumption originates from transport [1,2]. It is reported that urban overheating is detected in more than 400 major cities [3]. Most buildings are uninsulated or not insulated perfectly [4–7]. Moreover, insulation is important not only for the buildings but for the building service systems as well, like pipes transporting hot fluid for example in power plants or for district heating channels [8–9]. The thermal insulation of pipings is also very important both to increase thermal efficiency and to prevent energy loss. It is best to use high-temperature thermal insulations such as mineral wools, fiberglass or nowadays aerogels. These insulations should stand elevated temperatures of at least up to 300 °C, however, these heat treatments can also be understood from the point of view of the aging of the material to predict the life-time of the insulation. In most power plants, fiberglass or rock wool insulation is currently used to insulate these pipes. The properties of these materials deteriorate significantly over the years, for example, by crumbling with a decrease in thickness, therefore they can suffer changes in their thermal insulation capability [10]. It is reported that silica-aerogel materials behave as excellent thermal insulators even at high temperatures [11,12]. The role of thermal insulations for pipes is not only heat loss reduction, but physical and fire protection and preventing condensation. To make the requirements for insulating coatings clearer, let us take a closer look at the functions they perform [13–15]: a) reduction of heat loss, the higher the thermal conductivity of the pipe material, the greater the heat loss b) prevention of water condensation, therefore prevention from corrosion c) protection against thermal burns in direct contact with a heat conductor. As it is mentioned above, new-generation aerogels with metallic contaminants which stand high temperatures, such as Slentex and Pyrogel can be well applied for insulating district heating systems as well as can be used by power plants and the industry. Silica aerogel is a silicon dioxide-

* Corresponding author.
E-mail address: alakatos@eng.unideb.hu (Á. Lakatos).

https://doi.org/10.1016/j.tsep.2023.101906
Received 30 January 2023; Received in revised form 6 May 2023; Accepted 9 May 2023
Available online 12 May 2023

based material, which is a loose, dendritic network of silicon atoms. The aerogel thermal insulation blanket is a flexible composite material, which is aerogel embedded in a glass fiber network. They have high porosity (80–99.8%), very low density (4–220 kg/m^3) and excellent thermal conductivity (0.013–0.023 W/mK). These new-generation aerogels used for higher temperatures contain a significant amount of metals such as alumina, iron, calcium, titanium and magnesium as well as the bulk amorphous SiO_2 or they can also contain carbon. The addition of metals can enhance their thermal stability significantly [15–18]. Aerogels have much better thermal insulation capability than conventional insulations, such as glass wool used for pipes [19–22]. Aerogels can also be efficiently used for windows, historical buildings, as well as for plasters [23–25]. Moreover, In Ref. [26] a paper presents another possible application of aerogels, as an addition to plasters. With the mixture a high performance thermal insulation render can be reached. A similar investigation and research are presented by Ganobjak, showing a possible use of the aerogel render for historical buildings, see Ref. [27]. This case study also supports the applicability of the aerogel thermal insulations. Additionally, researchers present the key findings of EFFESUS project. This EU project presents the possible application of aerogels as a blown-in insulation [28]. Firstly, in contrast to the beforementioned papers where the thermal insulation capability was tested at common temperature ranges, we went further and examined the possible application of these aerogel materials at elevated temperatures. Generally, the production of the aerogel insulation blankets is expensive and hard. Furthermore, in this, paper comprehensive and gap-filling investigations are presented that were executed on two different types of aerogel thermal insulations containing metal additives such as Slentex and Pyrogel. These materials are said to be proper insulators for pipes transporting hot steam for district heating systems or power plants. Under these circumstances, they can meet a temperature range up to 250 °C. These temperatures can cause changes in the thermal properties of the insulations, such as their thermal conductivity and specific heat capacity. These changes may occur from the surface and the structural modifications of the materials. To reveal them firstly we annealed the samples at 150 and 250 °C for one day separately and after this their thermal conductivities and specific heat capacities were measured. To visualize the possible changes in the surface morphology optical microscope (OM) as well as scanning electron microscopy (SEM) images were taken. These photos were completed with hydrophobic experiments. To see the possible changes in the structure differentiated scanning calorimetry (DSC) and x-ray diffractometry (XRD) measurements were executed. The thermal conductivities and specific heat capacities were measured with Netzcsch HFM 446 small instrument. The key hypotheses of the article are as follows: a) After visual inspection, does the look of the material change as a result of heat treatment in air environment? b) Does the surface morphology of the material change as a result of heat treatment? c) Is there a change in the structure of the material and how does this affect the thermal parameters of the material, such as the thermal conductivity and specific heat? d) Are these materials suitable for use in raised-temperature environments? The novelty of the paper should be found in the following. The tested Slentex and Pyrogel aerogel insulations are relatively new, and can be widely used also in the industry because their production is well known. Thermal annealing serves also as the thermal ageing of the samples, it is very important because it can predict the life-time and the applicability limit of the insulation. We investigated and treated them in the same environment and we revealed their different behaviour. Another novelty of the research can be found in its interdisciplinarity. In the paper beside the general building physical investigations (thermal conductivity and specific heat) very deep solid state physical examinations were also executed, to reveal the background of both the changes and processes which are related to each other.

2. Materials and methods

2.1. The materials

In our laboratory we investigated two metallic added aerogels such as slentex and Pyrogel. Slentex is the second generation of conventional type Spaceloft aerogel. It has white color, A2-s1, d0 fire classification and approximately 190 kg/m^3 density. Pyrogel has a greenish-grey color, and contains a significant amount of carbon, enables its use as pipe insulation. Its density and fire safety category is similar to the above-mentioned one. Both of them are high-performance and efficient thermal insulations, slim and non-combustible [29].

2.2. Microscopic investigations with an optical microscope and scanning electron microscope

To visualize the surface morphology of the samples microscopic images were taken with both optical and scanning electron microscopes. To reveal the structure of both the as-received and annealed samples microscopy images were taken. Images from the bulk samples were taken with a camera with 20x magnification. A scanning electron microscope (SEM) was applied to study the morphology of the fibers and the blankets in more detail. A dual beam microscope type Thermo Fisher Scientific-Scios 2 (FIB-SEM, Waltham, MA, USA) was used to examine the samples. To study the composition of the samples the microscope was equipped with Bruker type detector for energy dispersive X-ray spectroscopy (EDS) analysis. Since the samples were electrically insulating, the microscope was operated at low voltage. The advantage of using a low accelerating voltage (1–2 keV) is that the secondary electrons generated near the surface can easily escape and in this way we can increase the yield. The increased yield increases the probability of collecting the electrons needed for imaging, thereby providing the opportunity to examine insulating samples without the application of gold coating, which may modify the surface morphology [30,31]. With an optical microscope, the surface of the samples was also analysed through hydrophobicity experiments [24,31].

2.3. Thermal conductivity and specific heat capacity measurements with NETZSCH 446 heat flow meter

With Netzsch Heat Flow Meter 446 small equipment we analysed the two most important thermal parameters of thermal insulation materials such as specific heat capacity and thermal conductivity. With this equipment, we analysed both the as-prepared and heat-treated samples. Three samples, each with a 20 cm × 20 cm base area were tested. The thermal conductivities were characterized between mean temperatures of 10 and 40 °C with 10 °C steps and under 20 °C temperature difference each. After the calibration of the equipment, the accuracy can be lower than 2%. Furthermore, the thermal conductivities were also measured at 20 °C mean temperature after applying 1, 4, 8 and 15 kPa load. The importance of testing the thermal conductivities of the fibrous samples under loads is the following. During the application of flexible insulations for pipes they were firmly fixed with a net which can compress them. The specific heat capacities were evaluated at 10, 24 and 40 °C. Specific heat tests can also be named as Cp measurements. The specific heat capacity of the samples can be determined with the step heat method. This measurement is much more accurate than the Cp measurement of the DSC because the whole blanket with realistic sizes is tested, while in DSC only small ground samples with about 10–20 mg are examined. The measurements were executed through the roles of ASTM C518 and ISO 8301 standards. After the measurement rows the average values of both the thermal conductivities and the specific heat capacities were calculated [24,31], in the figures the estimated deviances are also represented.

For the thermal conductivity measurements, the following equation is used (Eq. (1)):

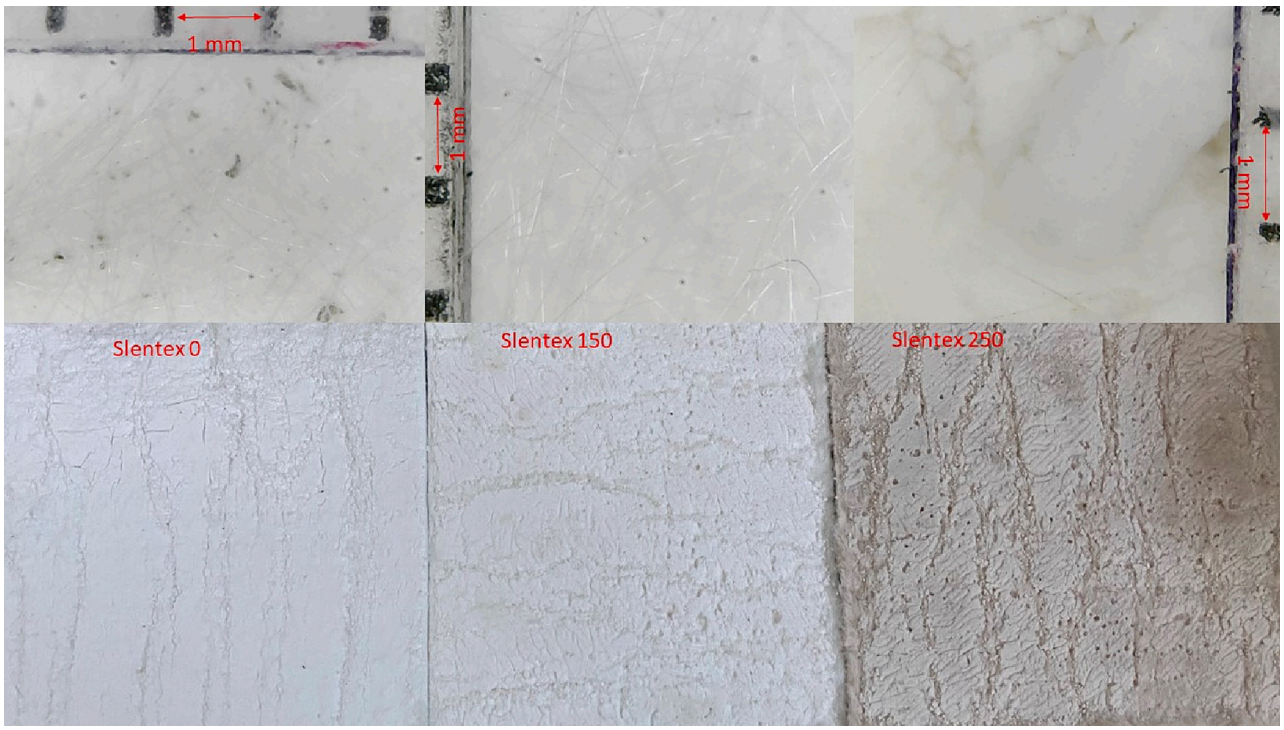

Fig. 1a. Optical microscope and a photo image of the as-received and heat-treated samples – Slentex.

$$l = N \times V \times (Dx/DT) \quad (1)$$

where λ is the thermal conductivity, V is the voltage output, N is the calibration factor, Δx is the specimen thickness and ΔT is the temperature step.

During a specific heat test, the HFM measures "steps" instead of "setpoints" (setpoints are common for thermal conductivity test measurements). To define the specific heat capacity the following formula is used (Eq. (2)):

$$Cp = N \times A \times (Q - Q_E)/m \times \Delta T \quad (2)$$

where m is the specimen mass, Q is the total energy absorbed by the plates, Q_E is the total energy absorbed by the plates and the specimen and A is the specimen area. The Cp value (specific heat capacity) of thermal insulation materials can be measured with Netzsch HFM 446. The heat flux signs are collected and integrated. It is recommended to increase specimen mass and the temperature step to try to get a high total energy absorbed by the plates and the specimen. The bigger this is compared to the total energy incorporated by the plates (empty stack correction) the better is the reproducibility and accuracy of the method. This means masses below 20 g are hard to measure in general. For an overall Cp validation a step size of 10 to 20 K is used. An empty stack correction was performed prior to a specific heat test (Cp measurement).

2.4. Differentiated scanning calorimetry

Differentiated scanning calorimetry is a well-known method to analyse both the contaminants and the possible changes in the samples after heat supply. Therefore we tested ground samples from the whole blankets with about 10–20 mg mass. The measurement order was the following: In a nitrogen atmosphere with 40 and 60 ml/min flow (ambient and protective) the samples were heated from 30 to 350 °C with a 10 °C/min heating rate in a concave Al pierce lid and then the DSC sign (in MW/mg) was registered in the function of the temperature. From the DSC grams the possible energetic and structural changes were evaluated [31]. The equipment works according to ISO 11357, ASTM E793, ASTM D3895, ASTM D3418 and DIN 51004 standards.

2.5. X-ray diffractometry investigations

To obtain crystallographic information from the un-annealed and annealed samples the X-ray diffraction (XRD) measurements were performed by Rigaku SmartLab diffractometer using CuK-alpha irradiation with wavelength of α = 0.154 nm. Bragg–Brentano focusing geometry was applied to scan the samples in 10-80° theta–2theta range to identify the possible changes of crystalline phase in the samples. The X-Ray tube was operated at 45 kV with 200 mA current. [31].

3. Results and discussion

3.1. Thermal annealing of the samples

We heat-treated, thermally aged three pieces of both Slentex and Pyrogel samples for 150 and 250 °C temperatures for one day in a Venticell 111 drying equipment in air. This equipment gives the opportunity to dry, desiccate or heat treat samples up to 300 °C. After the heat treatments, the following examinations were executed.

3.2. Analysis of the surface morphology

The change in the surface morphology of the samples after heat treatments was followed by microscopic methods. The general surface morphology of fiber reinforced aerogels can be imagined as a randomized network of fibers covered with the aerogel granules with different sizes. Due to thermal annealing the surface morphology can be changed. The modification can be resulted by the surface oxidation, chemical reactions, coalescence or disintegration of grains [32]. To reveal these we executed the following tests.

3.2.1. Optical microscopic investigations of the samples

Firstly, by visual inspection, we determined that the color of the samples belonging to Slentex got darker after thermal annealing (see Fig. 1a bottom part), which can be the result of the surface oxidation of

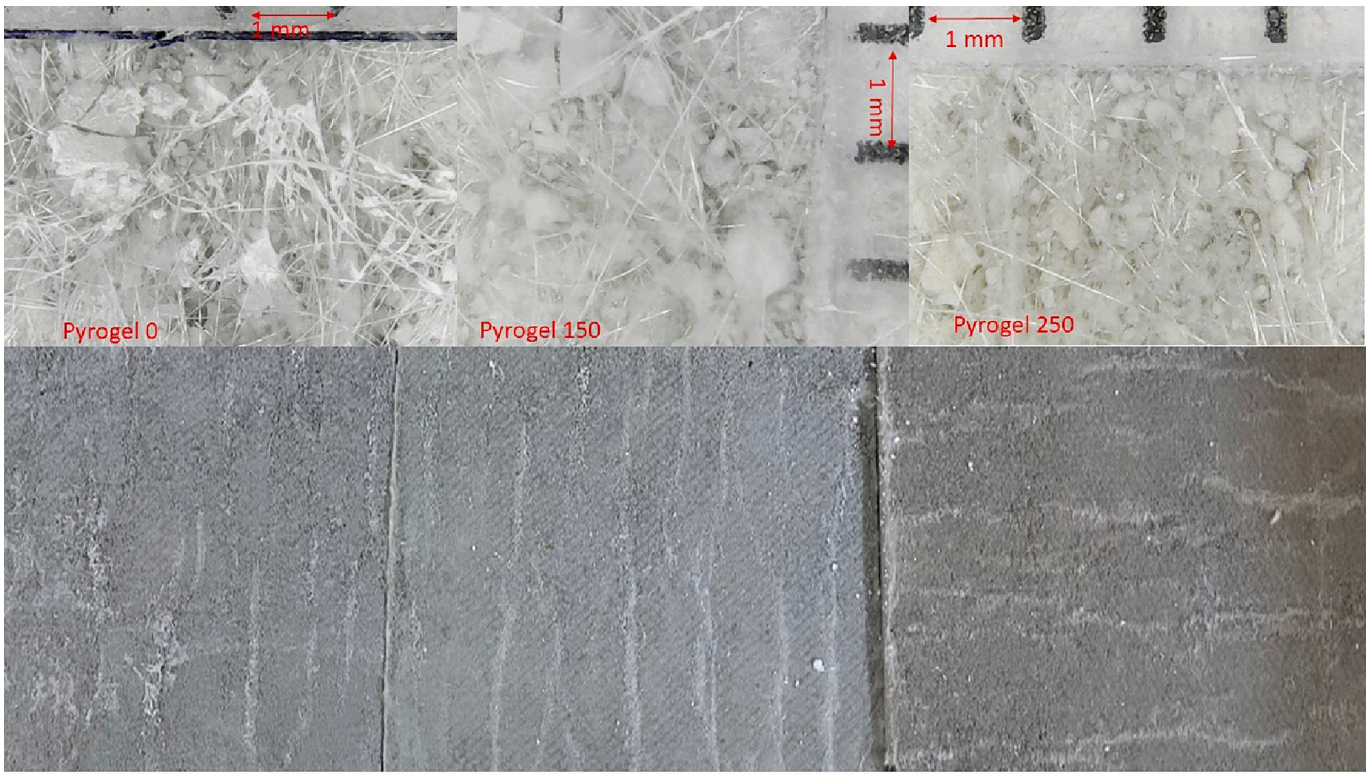

Fig. 1b. Optical microscope and a photo image of the as-received and heat-treated samples – Pyrogel.

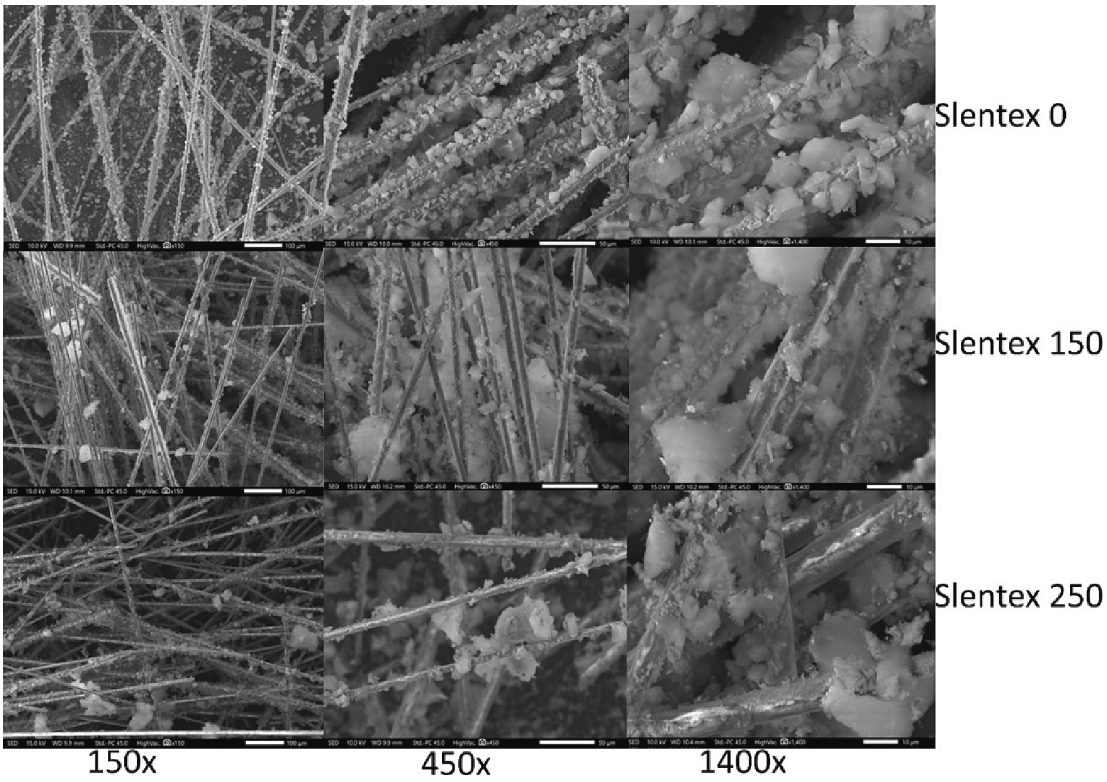

Fig. 2a. Scanning electron microscope image of the as-received and heat treated samples – Slentex.

the sample. After thermal annealing, the samples became less flexible and more rigid. With an optical microscope with about 20x magnification we detected that the fibers were covered with aerogels for both the un-annealed and annealed ones at 150 °C (Slentex 0 and 150), while for the sample annealed at 250 °C for 1 day we noticed both the separation of the aerogel particles from the fibers and their integration, it is visible in the right top image of Fig. 1a.

From the visual inspection of the Pyrogel samples, we detected only a

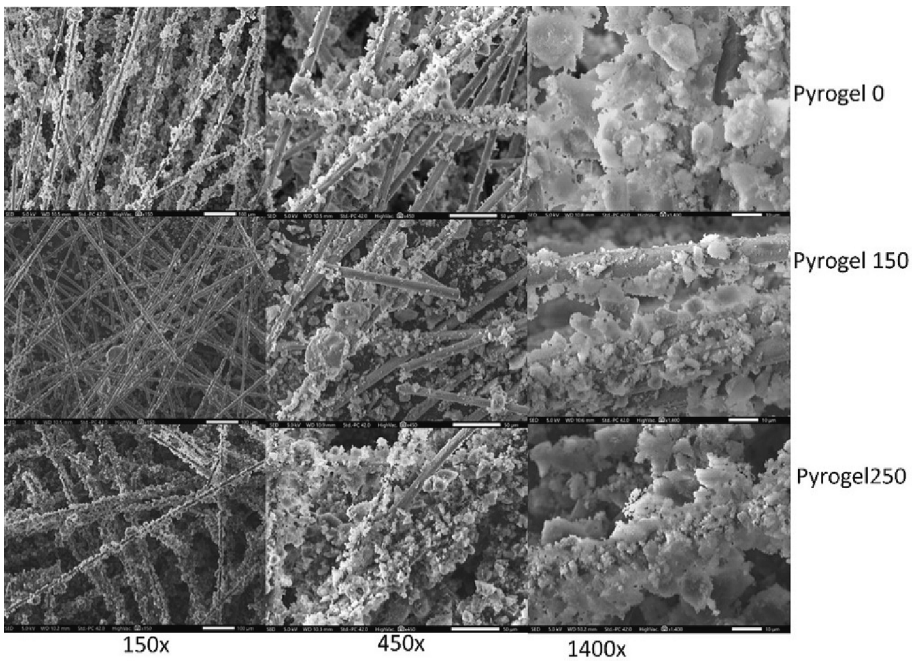

Fig. 2b. Scanning electron microscope image of the as-received and heat-treated samples – Pyrogel.

Element	Mass%	Atom%
C	15.73±0.30	24.70±0.47
O	42.46±0.59	50.05±0.69
Na	0.12±0.04	0.10±0.03
Mg	0.19±0.04	0.15±0.03
Al	4.37±0.12	3.05±0.08
Si	22.26±0.27	14.95±0.18
K	0.34±0.05	0.16±0.02
Ca	14.52±0.28	6.83±0.13
Total	100.00	100.00

Slentex - RED field

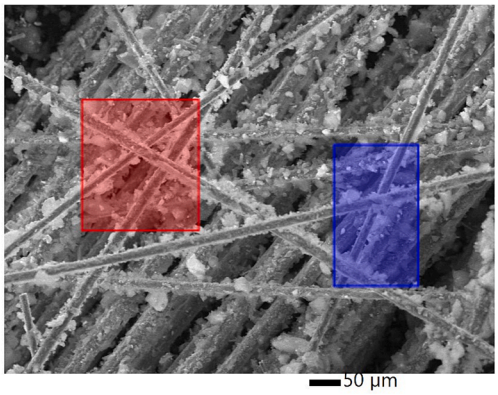

Element	Mass%	Atom%
C	13.70±0.29	21.94±0.46
O	42.38±0.59	50.93±0.71
Na	0.23±0.04	0.20±0.04
Mg	0.18±0.04	0.14±0.03
Al	4.81±0.13	3.43±0.09
Si	23.42±0.28	16.03±0.19
K	0.29±0.05	0.14±0.02
Ca	14.99±0.29	7.19±0.14
Total	100.00	100.00

Slentex - BLUE field

Fig. 3a. Results of the composition analysis measurements – Slentex.

Element	Mass%	Atom%
C	15.75±0.39	24.37±0.60
O	43.84±0.68	50.94±0.79
Mg	0.16±0.04	0.12±0.03
Al	3.51±0.13	2.42±0.09
Si	27.13±0.36	17.96±0.24
Ca	6.81±0.24	3.16±0.11
Ti	1.73±0.14	0.67±0.06
Fe	1.07±0.17	0.35±0.06
Total	100.00	100.00

Pyrogel - RED field

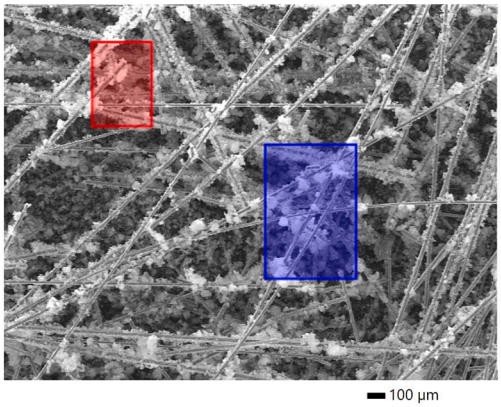

Element	Mass%	Atom%
C	20.70±0.42	30.80±0.62
O	42.41±0.66	47.39±0.74
Na	0.32±0.05	0.25±0.04
Mg	0.21±0.04	0.15±0.03
Al	2.98±0.12	1.97±0.08
Si	24.98±0.33	15.90±0.21
Ca	6.09±0.22	2.72±0.10
Ti	1.42±0.13	0.53±0.05
Fe	0.89±0.15	0.28±0.05
Total	100.00	100.00

Pyrogel - BLUE field

Fig. 3b. Results of the composition analysis measurements – Pyrogel.

color change after annealing the samples at 250 °C for 1 day, it was possibly arising from the oxidation. It is interesting that by magnifying the surface with 20x a slight crushing of the grains can be noticed (see Fig. 1b).

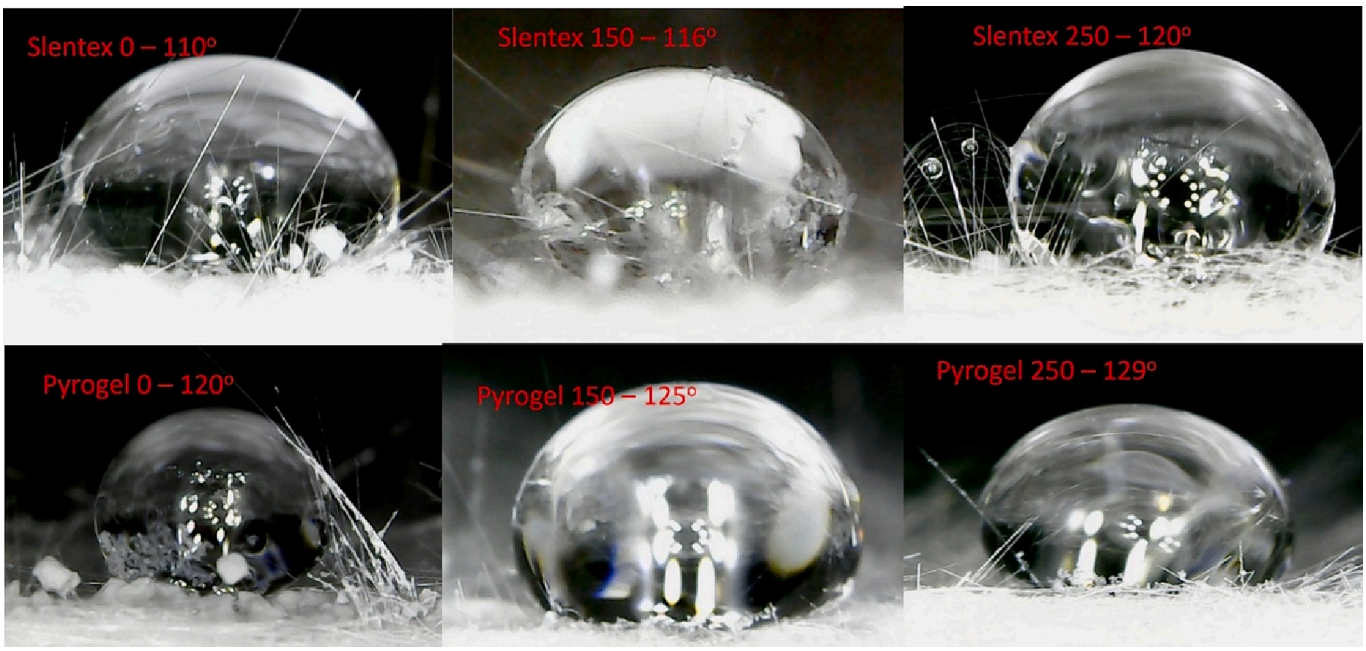

Fig. 4. The hydrophobic experiments of the samples.

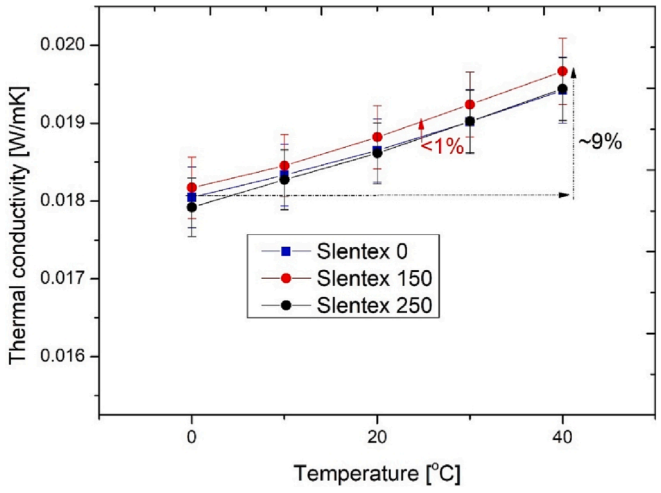

Fig. 5a. Measurement mean temperature vs. thermal conductivities of the Slentex samples.

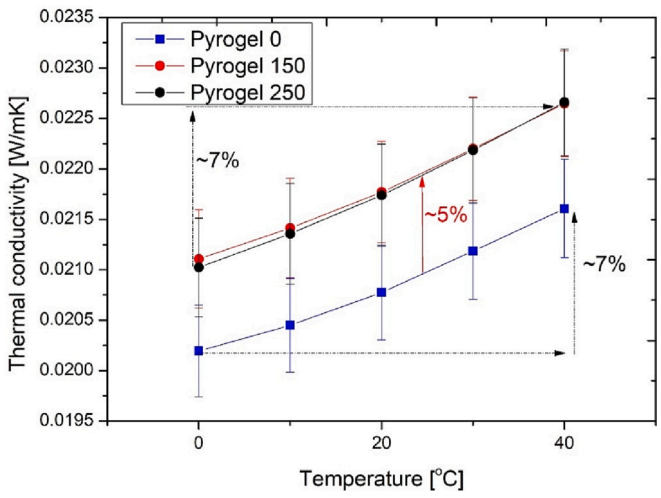

Fig. 5b. Measurement mean temperature vs. thermal conductivities of the Pyrogel samples.

3.2.2. Scanning electron microscope investigations

With the above-mentioned SEM equipment, we examined the surface morphology of the samples deeper in three steps. We present the results with three different magnifications (150, 450 and 1400x). SEM imaging is an excellent method to analyse the surface morphology of aerogel samples [33–36]. From Fig. 2a we can further confirm the above-mentioned process which was the detachment of grains from the fibers and their coalescence. A similar effect was also detected earlier on a different fiber reinforced aerogel presented in Ref. [32].

From Fig. 2b we can also observe some separation of the grains. Based on the scanning electron microscopic examination results of the morphology of the insulating materials, it can be established that internal structural changes occur on the surface of the insulating layers containing aerogel (Slentex, Pyrogel) due to the heat load caused by the heat treatment. During the modification, the aerogel particles attached to the glass fibers flake off, and an increase in particle size could be observed, which might have caused a change in both the specific heat capacity and the thermal conductivity of the materials.

From Figs. 3a and b we can state that the main components of both the Slentex and the Pyrogel samples are silicon and oxygen (possibly SiO_2), while Slentex further contains Na, K, Ca, Mg and Alumina. Moreover, for Pyrogel the further contaminants are C, Fe, Ti, Na, Al, Mg and Ca (see Figs. 3a and b). Metal contaminants can lead to the high thermal stability of these kinds of aerogels.

3.2.3. Examination of the hydrophobic properties

Another method through microscopy to analyse the surface of the materials is the hydrophobic test. We call a surface hydrophobe if the contact angle between the solid surface and the water droplet is greater than 90° [37]. For this, in Fig. 4 we collected the contact angle test results of the samples for both un-annealed and annealed ones, belonging to Slentex as well as to Pyrogel. One can see that the contact angle is increasing in both cases after heat treatments. It also depicts modifications in the surface morphology of the samples. From the contact angles, we can estimate an approximate 5% and 8 % increase in both cases after

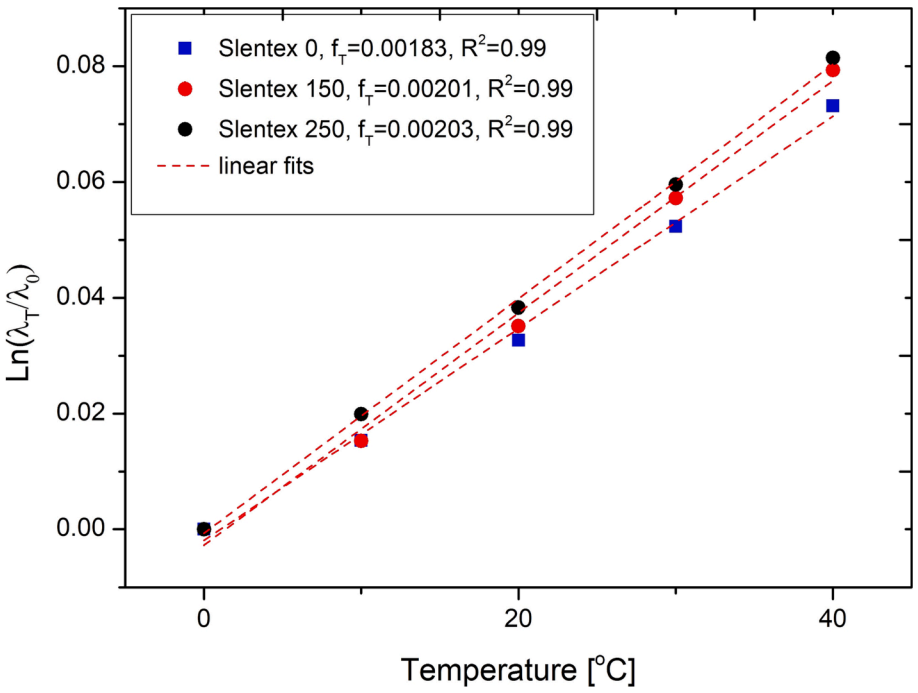

Fig. 6a. The fitted temperature conversion coefficients (f_T) for Slentex.

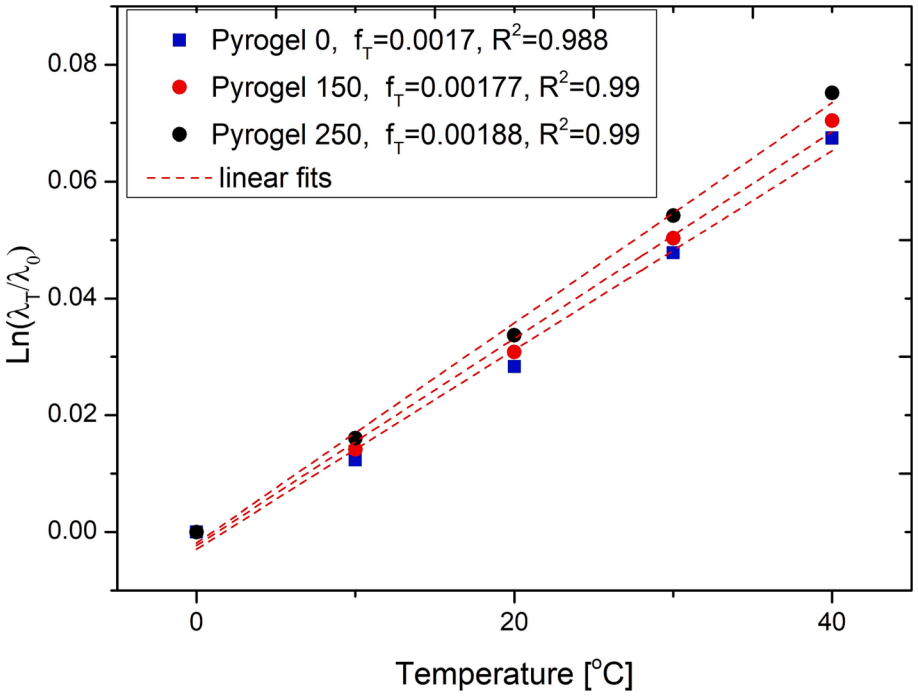

Fig. 6b. The fitted temperature conversion coefficients (f_T) for Pyrogel.

thermal annealing at 150 °C and 250 °C respectively. It can also predict an increasing specific surface area caused by the union and fragmentation of aerogel particles for the Slentex and the Pyrogel respectively. Moreover, we can also explain the increase in the contact angle with both the oxidation of the surface and the microstructural changes (justified by microscopes), making the surface more hydrophobic. Figs. 5a and b.

3.3. Results of thermal conductivity measurements

3.3.1. Thermal conductivity versus temperature

With t Netzsch 446 HFM thermal conductivities at different mean temperatures from 0 to 40 °C with 10 °C steps and 20 °C temperature difference were characterized. We measured both the un-annealed and the annealed samples. From the measurements we can state that the Slentex aerogel is a stable thermal insulation from the heat-treatment (at 150 and 250 °C) point of view because its thermal conductivity remains constant, and the change is within the accuracy of the equipment (<2%).

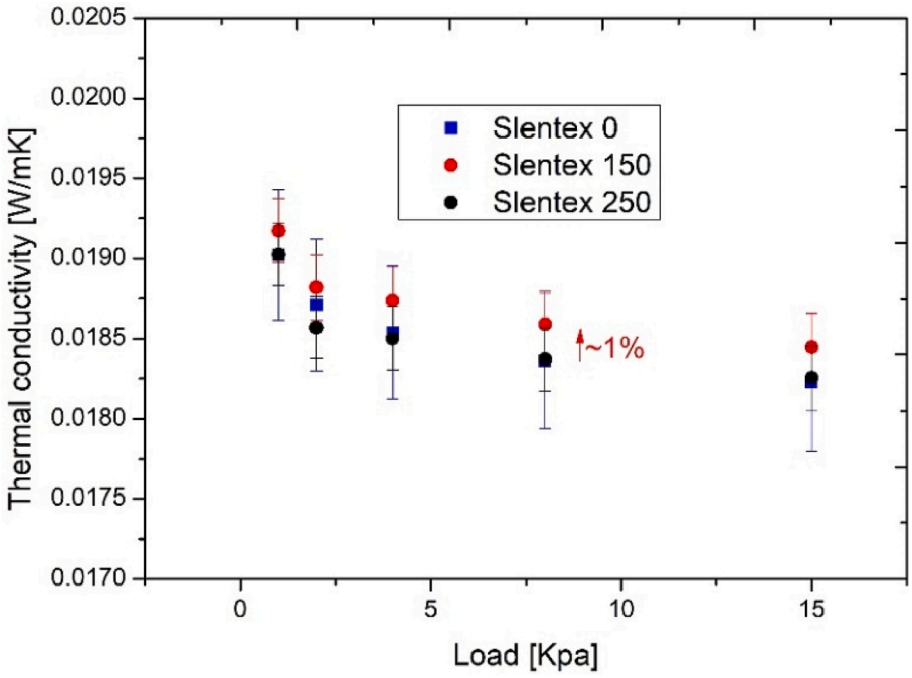

Fig. 7a. Applied load versus thermal conductivities of the Slentex.

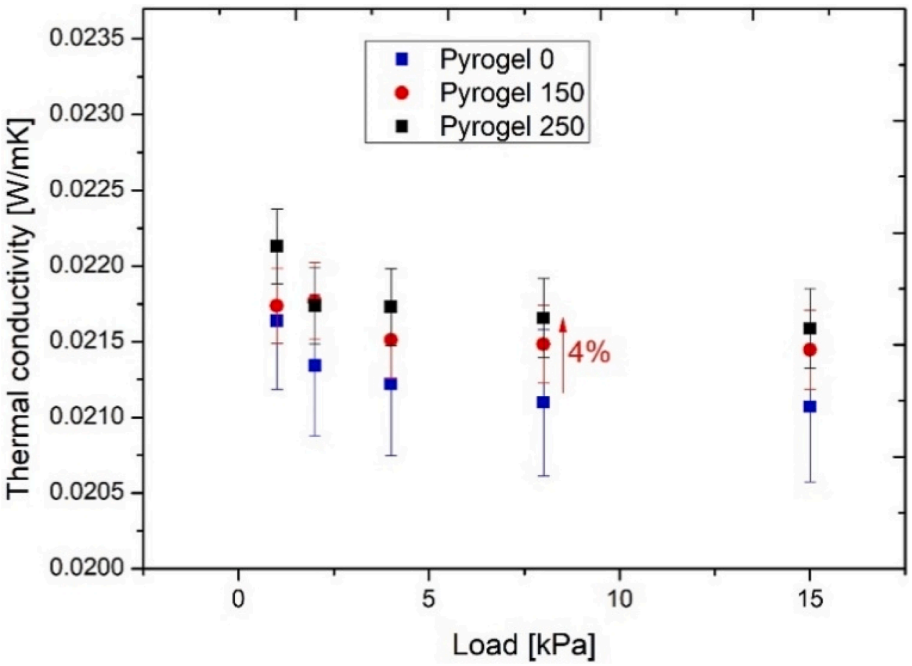

Fig. 7b. Applied load versus thermal conductivities of the Pyrogel samples.

But it is worth mentioning that the thermal conductivity is sensitive to the mean temperature because between 0 and 40 °C it changes by about 9% independently from the thermal annealing. Furthermore, by analysing the thermal conductivity profiles of Pyrogel we can state that after thermal annealing the samples at 150 °C the thermal conductivity changed by about 5%, and the same change was found for the samples annealed at 250 °C. From the temperature sensitivity test, we can conclude that for both the un-annealed and the annealed samples the thermal conductivity between 0 and 40 °C changes by about 7%. To understand the results we should go further and we have to investigate other thermal and structural parameters. Compared to sources from the literature, we can state that these thermal conductivity values (0.016–0.023) are within the range of the thermal conductivities belonging to fibrous aerogels [11,21,23,27].

From Figs. 6a and b by using the rules of ISO 10456 standard the temperature's effect on the thermal conductivity of the samples can be reached and it is named as the temperature conversion coefficient (f_T). The standard gives the calculation method (Eq. (3) to (5) for reaching the interrelation between the thermal conductivity at an arbitrary mean temperature and the value of the thermal conductivity measured at 0 °C temperature. Between two temperatures (T_j and T_0) one can estimate the temperature conversion coefficient representing the sensitivity of the

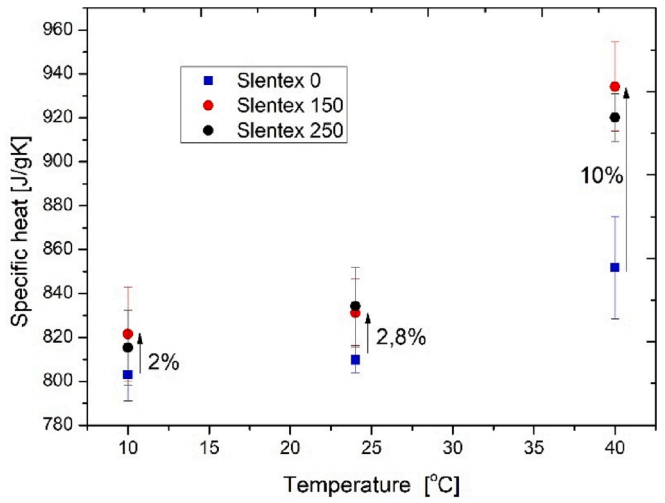

Fig. 8a. The Cp measurement results of Slentex.

thermal conductivity to the temperature by using F_T conversion factor. Figs. 7a and b.

$$F_T = \exp(f_T \times (T_j - T_0)) \tag{3}$$

$$l_T = l_0 \times F_T \tag{4}$$

By using the logarithm natural the downer equation can be reached:

$$\ln(l_T/l_0) = f_T \times DT \tag{5}$$

It is interesting that, while the thermal conductivity factors changed little or not at all, the f_T values did with about 10% by annealing the samples at 250 °C.

It was presented earlier, that load applied on fibrous insulation materials during the thermal conductivity measurements can change the density, therefore the thermal conductivity, too, because the equipment squeezes the excess air out of the fibers of the sample [38,39]. For this purpose we used the heat flow meter, which allows measuring the thermal conductivity after applying forces/loads on the samples. At 20 °C mean temperature loads with 1, 2, 4, 8, and 15 kPa were applied to the samples and their thermal conductivities were registered. In general, the measured thermal conductivities decreased with the applied load for both types of aerogels in all cases (un-annealed/annealed). We have to mention that the values belonging to Slentex due to the heat treatments did not change while for the Pyrogel a 4% change was deduced after annealing at 150 and 250 °C.

The limitation of the measurements can be defined by the uncertainty. This can be given as:

$$(U\_TC)^2 = (\delta\lambda/\lambda)^2 = (\delta N/N)^2 + (\delta E/E)_S^2 + (\delta E/E)_C^2 + (\delta L/L)_S^2 + (\delta L/L)_C^2 + (\delta\Delta T/\Delta T)_S^2 + (\delta\Delta T/\Delta T)_C^2 \tag{6}$$

where $\delta\lambda/\lambda$ is the relative standard uncertainty of the thermal conductivity, $\delta R/R$ is the relative standard uncertainty of the thermal resistance, $\delta N/N$ is the estimated relative uncertainty of the calibration factor, $\delta E/E$ is the estimated relative uncertainty of the heat flux meter, $\delta L/L$ is the estimated relative uncertainty of the thickness transducer, $\delta\Delta T/\Delta T$ is the estimated relative uncertainty of the temperature difference across the specimen, S is the sample measurement, C is the calibration measurement.

3.4. Specific heat capacity measurement results and theoretical models

The specific heat capacities for all the samples were measured at 10, 24 and 40 °C. From the measurements belonging to the Slentex aerogel, we can state that with increasing temperature the specific heat capacity of the samples is increasing. However, at 40 °C one can deduce a 10% change in the Cp value after thermal annealing at 150 and also for 250 °C. Figs. 8a and 8b represent the results. For the Pyrogel insulation, we found a significant change in the specific heat capacity at both 24 and 40 °C after thermal annealing. The Cp value at 24 °C goes up by 5 and 8% after thermal treatments at 150 and 250 °C, while at 40 °C the Cp value jumps up by about 11% after the heat treatment of samples at 250 °C. The specific heat capacity of the samples also reflects the crystal structure of the samples (oxidation, amorphous or crystalline). So to understand these results we had to expand our research with the

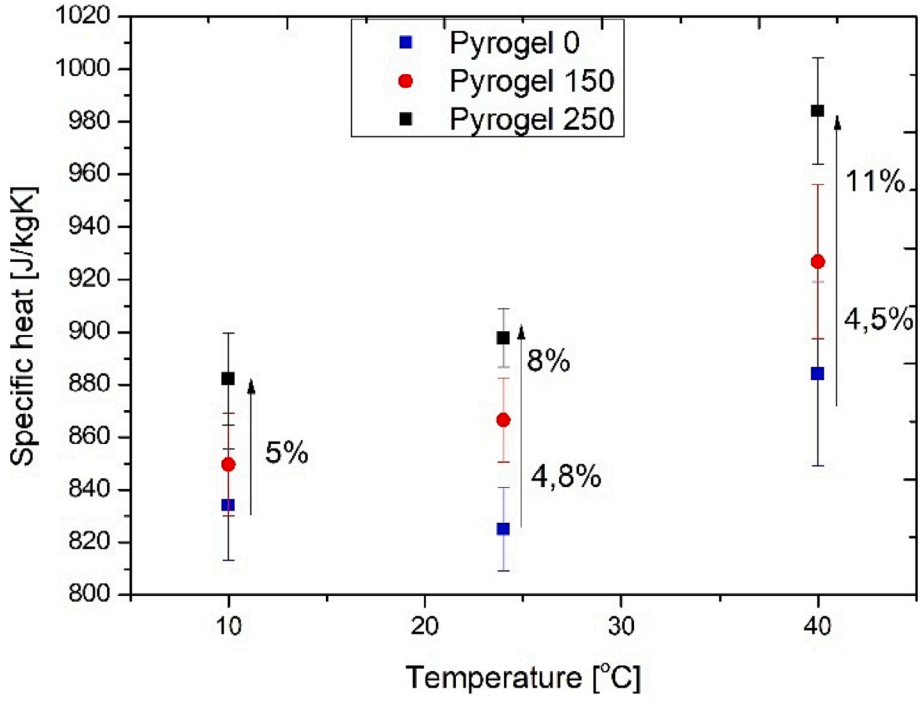

Fig. 8b. The Cp measurements results of Pyrogel.

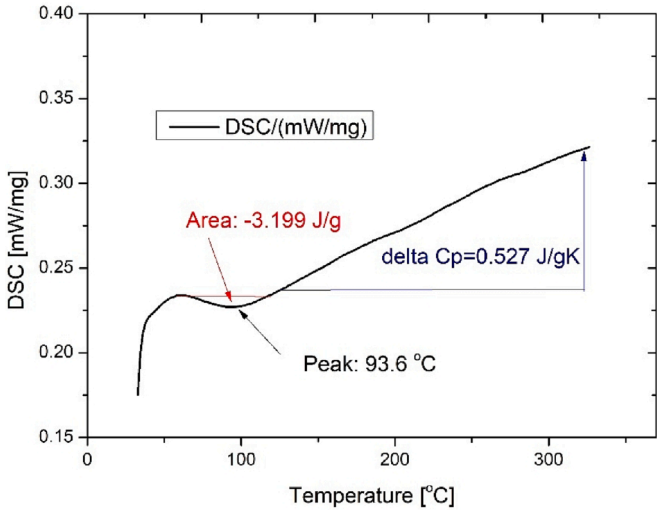

Fig. 9a. DSC profile of Slentex.

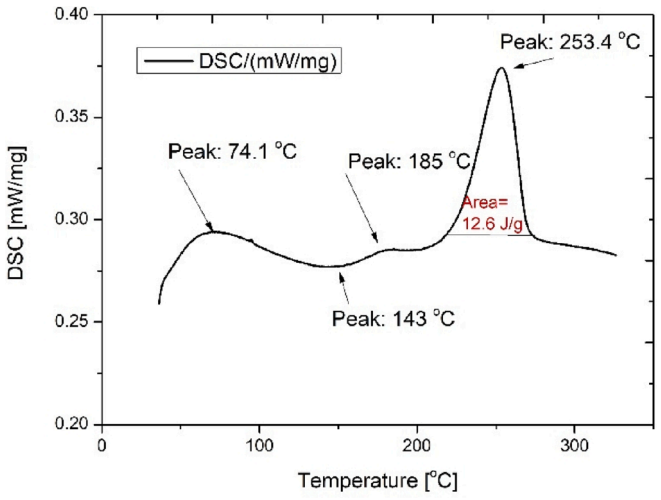

Fig. 9b. DSC profile of Pyrogel.

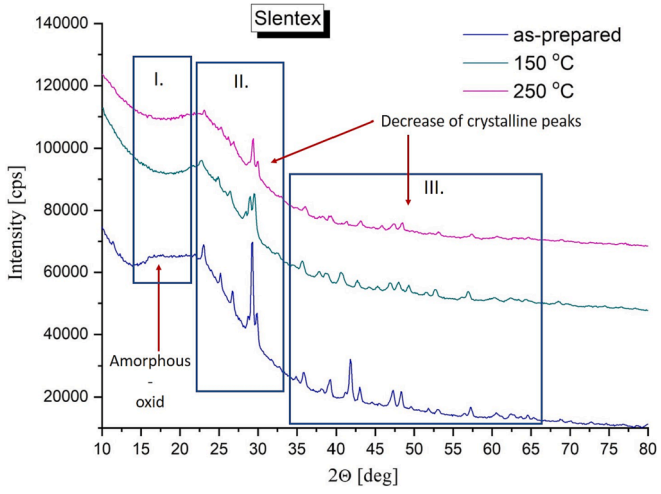

Fig. 10a. XRD profile of Slentex.

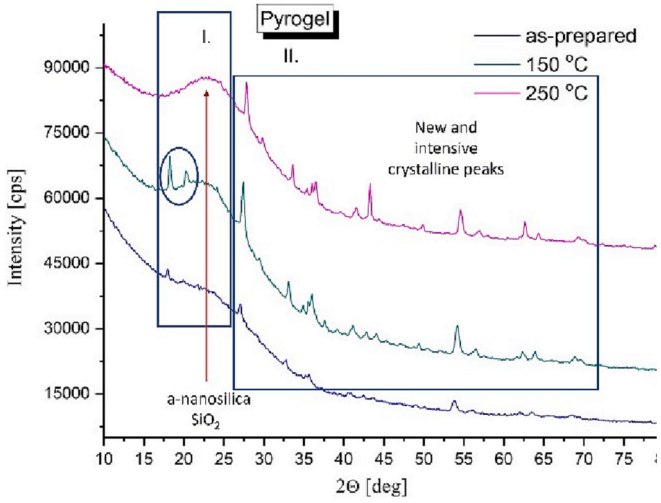

Fig. 10b. XRD profile of Pyrogel.

examinations of the material's structure.

For all specific heat capacity investigations at least three samples were tested, and from the test results the averages with the estimated deviances are plotted.

3.5. *Differentiated scanning calorimetry*

Thermal insulation materials generally have an amorphous structure, containing significant amount of oxides, such as silicon-oxide or amorphous silica nanoparticles. Due to the temperature rise the amorphous structure can be restructured or crystallized, recrystallized [11,12]. With the crystallization process the thermal conductivity and the specific heat capacity of the materials can increase and deteriorate their thermal insulation capability. By using Netzsch Sirius 3500 differentiated scanning calorimeter we have analysed the thermal response of the powder of both samples after grinding. A small amount (10 mg) from the samples (Slentex, Pyrogel) was inspected between 30 and 350 °C with 10 K/min heating rate in nitrogen gas. For the Slentex aerogel, we found that the profile has an initial part until 70 °C, where one can possibly deduce the region of the glass transition or residual water. After this a valley can be found with the deepest point at 93 °C which can be attributed with a crystallization of the amorphous structure with an enthalpy of −3.2 J/g, see Fig. 9a. Over this, dehumidification-decomposition can be expected [40]. One can deduce here a change in the specific heat capacity with about 527 J/kgK value.

Similar results can be found presented in Fig. 9b for Pyrogel between 30 and 70 °C which belongs to the glass transition region, then a slight peak is observable possibly representing a light crystallization (143 °C). It is also visible from Fig. 8b that first a small melting peak by 185 °C, then a strong melting peak from 220 to 270 °C can be found. Possibly it can be attributed to the melting of a polymeric compound with about 12.6 J/g melting enthalpy. During the calorimetric examination of partially crystalline polymers, after the crystallization transition, a first-order phase transformation takes place in the higher temperature range, during which the formed crystal structure becomes completely amorphous again. This transformation is the melting of the polymers, which appears as an endothermic peak on the DSC curve. When evaluating the curve, the area under the peak is proportional to the enthalpy change that occurred during the melting of the sample. The temperature value corresponding to the highest point of the peak gives information about the melting temperature of the polymer, but it is not the same as the equilibrium melting point, since its value depends greatly on the test conditions and the history of the sample. It has to be mentioned that after this melting a significant amorphous part must remain inside the structure. A similar effect is presented in Ref. [41]. For the DSC

Table 1
The collection of the results.

	Slentex		Pyrogel	
	Results of thermal annealing	Meaning	Results of thermal annealing	Meaning
Visual inspection and optical microscope	change of the color, surface grains are growing	oxidation – surface modification	color change, the crush of grains	oxidation – surface modification
Scanning microscope	surface-grains are growing	surface modification	crush of grains	surface modification
Contact angle	contact angle is increasing	surface modification	contact angle is increasing	surface modification
Specific heat capacity	increasing	crystallization	increasing	changes = restructuring
DSC	crystallization, dehydration	structural change	melting peak at 250 °C	amorphous residue – structural change
XRD	crystallization – oxidation	structural change	increase to an amorphous peak, change	structural change
Thermal conductivity	remains constant	thermally stable	increase after thermal annealing at 150 °C	partially stable
Thermal conversion coefficient	increasing after thermal annealing at 150 and 250 °C by 10%	modification in structure	increasing after thermal annealing at 150 and 250 °C by 4 and 10% respectively	modification in structure

measurements two rows were executed on both sample pairs and their average was plotted.

3.6. Results of the XRD tests

From the X-ray diffraction measurements, we can conclude that the samples went through structural modifications after thermal annealing. Fig. 10a represents the XRD patterns of Slentex aerogel. The profile can be grouped into three regions. The first region belongs to the amorphous (oxid) region at about 15-22° [32,42]. One can observe from this part that due to thermal annealing, this plateau decreases, which means the restructuration of the sample. In the second region, 22-35° degree crystalline peaks can be observed belonging to the different orientations of the silicon oxide. After thermal annealing, the intensity of these crystalline peaks are decreasing. A similar change can be found in the third region. Regarding Pyrogel we can see two regions in Fig. 10b. The first region also belongs to the degrees of 15-25°. It is interesting that a broad peak belonging to the amorphous nano-silica (at 22°) becomes more observable after thermal annealing the samples with a possible interconnection with the melting of the polymer contaminant presented in Fig. 9b at 250 °C. While it is also noticeable that a doubled peak at about 17° grows out after thermal annealing at 150 °C and disappears after thermal annealing at 250 °C. It can be a crystalline peak that disappears due to the melting (burning). In the second region of the XRD pattern of Pyrogel, recrystallization can be observed. These peaks belong to SiO peaks with different crystal orientations [32,43–47].

3.7. The relationship between the results, the applicability limits

From the above-mentioned consequences, we created Table 1 to understand and generalize the key findings of the paper and to see the correlations among the results. This table could be very useful for researchers, designers, planners and decision makers.

It is also reported by Authors in Ref. [48] that the investigation of the thermal stability of elastic ceramic aerogels is very important from an applicability point of view. In Ref. [49] it is also presented that the use of aerogel blankets for high-temperature insulation is indispensable. These temperatures make changes in both the material and the thermal properties of the samples that must be followed experimentally [50], similarly as it is presented in this paper.

4. Conclusions

Slentex and Pyrogel insulations were heat-treated (aged) at 150 and 250 °C for 1 day, and their thermal, as well as physical properties, were measured. From the measurements, we revealed the modifications in both structures and thermal properties furthermore we explored the possible relations between them. As a novelty, we present measurement methods supporting each other to completely reveal the temperature-caused changes of the tested samples. As a result, we pointed out the visible and measurable surface and structural modifications for Slentex insulation. Microscope images proved the oxidation of the surface and the coalescence of the grains, while the DSC measurements denoted crystallizations and dehydration. The crystallization process was further justified by XRD experiments showing a decreasing amorphous peak as well as by the Cp measurements where we deduced about 10% change after annealing at 250 °C for 1 day. Despite all these, the thermal conductivities of the samples after thermal annealing remained constant. But it is worth mentioning that as a side result, we showed a strong temperature sensitivity of the thermal conductivity of the samples, with about a 9% increase between 0 and 40 °C mean temperatures for all three cases. For the Pyrogel, after both visual and microscopic investigations we found surface modifications in the samples after annealing at 250 °C. It was confirmed with scanning electron microscopy that the surface of the samples after heat treatment at 250 °C and for 1 day changed: the grains of the samples crumbled. It has to be mentioned that the hydrophobic experiments showed increasing contact angles for both Slentex and Pyrogel insulations due to surface oxidation. The specific heat capacities of the Pyrogel insulations changed strongly. But it was also mentioned that the DSC curve showed a strong melting peak at about 250 °C which can predict an amorphous residue in the structure and it was also found in XRD graphs. We showed about a 5% change in the thermal conductivity of the Pyrogel, after heat-treating the samples at 150 °C, while the change stopped and remained the same as the mentioned one due to the melting. Between 0 and 40 °C mean temperature the thermal conductivity increase by about 7%. Moreover, we showed that the temperature conversion coefficients changed with about 10% for the Slentex and with about 4 and 10% for the Pyrogel after annealing them at 150 and 250 °C respectively.

Declaration of Competing Interest

The authors declare that they have no known competing financial interests or personal relationships that could have appeared to influence the work reported in this paper.

Data availability

Data will be made available on request.

Acknowledgements

Project no. TKP2021-NKTA-34 has been implemented with the support provided by the Ministry of Innovation and Technology of Hungary from the National Research, Development and Innovation Fund, financed under the TKP2021-NKTA funding scheme.

References

[1] H. Saeed Khan, R. Paolini, P. Caccetta, M. Santamouris, On the combined impact of local, regional, and global climatic changes on the urban energy performance and

indoor thermal comfort—The energy potential of adaptation measures, Energy and Buildings 267 (2022) 112152.
[2] S. Taheri, A. Akbari, B. Ghahremani, A. Razban, Reliability-based energy scheduling of active buildings subject to renewable energy and demand uncertainty, Thermal Science and Engineering Progress 28 (2022) 101149.
[3] M. Santamouris, Recent progress on urban overheating and heat island research. Integrated assessment of the energy, environmental, vulnerability and health impact, Energy and Buildings 207 (2020) 109482.
[4] Moga, L., Moga, I., Heat loss coefficient influence on the energy performance of buildings, Indoor Air 2014 – Proceedings of the 13th International Conference on Indoor Air quality and Climate, (2014) ISBN 978-1-64339-731-5. 299-306.
[5] G. Grazieschi, F. Asdrubali, G. Thomas, Embodied energy and carbon of building insulating materials: A critical review, Cleaner Environmental Systems 2 (2021) 100032.
[6] A. Fateh, D. Borelli, F. Devia, H. Weinläder, Summer thermal performances of PCM-integrated insulation layers for light-weight building walls: Effect of orientation and melting point temperature, Thermal Science and Engineering Progress 6 (2018) 361–369.
[7] S. Cai, W. Zhu, L. Cremaschi, Study of the meso-structure and its impact on the thermal performance of closed-cell insulation with moisture ingress, Procedia Engineering 205 (2017) 2823–2830.
[8] M. Abujab, A. Abusafa, Optimal insulation's thickness of pipes in Variable Refrigerant Flow (VRF) system—An-Najah Child Institute as a case study, Energy Reports 8 (2022) 321–330.
[9] A. Yildiz, M. Ali Ersöz, Determination of the economical optimum insulation thickness for VRF (variable refrigerant flow) systems, Energy 89 (2015) 835–844.
[10] L. Ni, Y. Luo, C. Qiu, L.u. Shen, H. Zou, M. Liang, P. Liu, S. Zhou, Mechanically flexible polyimide foams with different chain structures for high temperature thermal insulation purposes, Materials Today Physics 26 (2022) 100720.
[11] Liu, H, Liu, J., Tian, Y., Wu, X., Li, Z. Investigation of high temperature thermal insulation performance of fiber-reinforced silica aerogel composites, International Journal of Thermal Sciences. Volume 183. 2023. 107827. ISSN 1290-0729.
[12] K. Wu, Q.i. Zhou, J. Cao, Z. Qian, B.o. Niu, D. Long, Ultrahigh-strength carbon aerogels for high temperature thermal insulation, Journal of Colloid and Interface Science 609 (2022) 667–675.
[13] O. Kaynakli, Economic thermal insulation thickness for pipes and ducts: A review study, Renewable and Sustainable Energy Reviews 30 (February 2014) 184–194.
[14] A. Bergea, B. Adl-Zarrabia, C.E. Hagentoft, Assessing the Thermal Performance of District Heating Twin Pipes with Vacuum Insulation Panels, Energy Procedia 78 (2015) 382–387.
[15] X. Zhou, H. Jin, Q. Shen, W. Huang, J. Li, Y. Liang, P. Mao, Y. Yang, S. Yun, J. Chen, Rapid preparation of Palygorskite/Al2O3 composite aerogels with superhydrophobicity, high-temperature thermal insulation and improved mechanical properties, Ceramics International 48 (22) (2022) 32994–33002.
[16] X. Xu, Q. Zhang, M. Hao, Y. Hu, Z. Lin, L. Peng, T. Wang, X. Ren, C. Wang, Z. Zhao, C. Wan, H. Fei, L. Wang, J. Zhu, H. Sun, W. Chen, T. Du, B. Deng, J. Cheng Gary, I. Shakir, C. Dames, C. Fisher, X.T. Zhang, H. Li, Y. Huang, X. Duan, Double-negative-index ceramic aerogels for thermal superinsulation Science 363 (6428) (2019) 723–727.
[17] Zhang, X., Wang, F., Dou, L., Cheng, X., Si, Y., Yu, J., Ding, B. Ultrastrong, superelastic, and Lamellar multiarch structured ZrO2–Al2O3 nanofibrous aerogels with high-temperature resistance over 1300 °C ACS Nano, 14 (11) (2020). 15616-15625.
[18] Z.Y. Li, H. Liu, X.P. Zhao, W.Q. Tao, A multi-level fractal model for the effective thermal conductivity of silica aerogel, J. Non-Cryst. Solids 430 (2015) 43–51.
[19] H.e. Liu, Z.-Y. Li, X.-P. Zhao, W.-Q. Tao, Study on unit cell models and the effective thermal conductivities of silica aerogel, J. Nanosci. Nanotechnol. 15 (4) (2015) 3218–3223.
[20] K. Ghazi Wakili, B. Binder, R. Vonbank, A simple method to determine the specific heat capacity of thermal insulations used in building construction, Energy Build. 35 (4) (2003) 413–415.
[21] R. Baetens, B.P. Jelle, A. Gustavsen, Aerogel insulation for building applications: a state-of-the-art review, Energy Build. 43 (4) (2011) 761–769.
[22] H.M. Danaci, N. Akin, Thermal insulation materials in architecture: a comparative test study with aerogel and rock wool, Environ Sci Pollut Res 29 (48) (2022) 72979–72990.
[23] Á. Lakatos, Stability investigations of the thermal insulating performance of aerogel blanket, Energy and Buildings 185 (2019) 103–111.
[24] Á. Lakatos, Thermal insulation capability of nanostructured insulations and their combination as hybrid insulation systems, Case Studies in Thermal Engineering 41 (2023) 102630.
[25] H.-P. Ebert, in: Aerogels Handbook, Springer New York, New York, NY, 2011, pp. 537–564.
[26] K. Ghazi Wakili, T.h. Stahl, E. Heiduk, M. Schuss, R. Vonbank, U. Pont, C. Sustr, D. Wolosiuk, D. Mahdavi, High Performance Aerogel Containing Plaster for Historic Buildings with Structured Façades, En. Proc. 78 (2015) 949–954.
[27] M. Ganobjak, S. Brunner, J. Wernery, Aerogel materials for heritage buildings: Materials, properties and case studies, Journal of Cultural Heritage 42 (2020) 81–98.
[28] E. Lucchi, F. Becherini, M.C. di Tuccio, A. Troi, J. Frick, F. Roberti, C. Hermann, I. Fairnington, G. Mezzasalma, L. Pockelé, et al., Thermal performance evaluation and comfort assessment of advanced aerogel asblown-in insulation for historic buildings, Build. Environ. 122 (2017) 258–268.
[29] http://www.aerogelszigeteles.hu/system/files/Spaceloft_DS_1.1.pdf.
[30] Erdman N., Bell D.C., Reichelt R.: Scanning Electron Microscopy. In Springer Handbook of Microscopy; Eds.: P. Hawkes, J.C. Spence. Springer International Publishing (2019). 229–318.
[31] Á. Lakatos, A. Csík, Multiscale Thermal Investigations of Graphite Doped Polystyrene Thermal Insulation, Polymers 14 (2022) 1606.
[32] A. Lakatos, A. Csik, A. Trnik, I. Budai, Effects of the heat treatment in the properties of fibrous aerogel thermal insulation, Energies 12 (10) (2019) 12102001.
[33] X. Yang, Y. Sun, D. Shi, J. Liu, Experimental investigation on mechanical properties of a fiber-reinforced silica aerogel composite, Mat. Sci. and Eng. A 528 (13-14) (2011) 4830–4836.
[34] Chakraborty, S., Pisal, A. A., Kothari, V. K., Rao, A. V. Synthesis and Characterization of Fibre Reinforced Silica, Aerogel Blankets for Thermal. Adv. in Mat. Sci. and Eng. 2016. Article ID 2495623.
[35] H. Nikpourian, R. Bahramian, Thermo-physical properties of multilayer super insulation: The role of aerogel blanket, Thermal Science and Engineering Progress 20 (1) (2020), 100751.
[36] Y. Liu, H. Wu, Y. Zhang, J. Yang, F. He, Structure characteristics and hygrothermal performance of silica aerogel composites for building thermal insulation in humid areas, Energy and Buildings 228 (2020), 110452.
[37] V. Novak, J. Zach, Study of the efficiency and durability of hydrophobization modifications of building elements, IOP Conf. Ser. Mater. Sci. Eng. 583 (2019), 012032.
[38] E. Dieckmann, R. Onsiong, B. Nagy, L. Sheldrick, C. Cheeseman, Valorization of Waste Feathers in the Production of New Thermal Insulation Materials, Valorization of Waste Feathers in the Production of New Thermal Insulation Materials Waste and Biomass Valorization 12 (2) (2021) 1119–1131.
[39] Lakatos, Á., Csík, A., Csarnovics, I. Experimental verification of thermal properties of the aerogel blanket, Case Studies in Thermal Engineering. 2021. 25. 100966.
[40] M.A. Hasan, S. Rashmi, A.C.M. Esther, P.Y. Bhavanisankar, B. Sherikar, N. Sridhara, A. Dey, 329 Evaluations of Silica Aerogel-Based Flexible Blanket as Passive Thermal Control Element for 330 Spacecraft Applications, Jou. of Mat. Eng. and Perf. 27 (2018) 1265–1273.
[41] Nagendra, B., Antico, P., Daniel, C., Rizzo, P., Guerra, G. Thermal shrinkage and heat capacity of monolithic polymeric physical aerogels, Polymer. Volume 210. 2020. 123073.
[42] Chen, X.Y., Hendrix, Y., Schollbach, K., Brouwers, H.J.H. A silica aerogel synthesized from olivine and its application as a photocatalytic support. Construction and Building Materials. Volume 248. 2020. 118709.
[43] T. Zhou, L. Gong, X. Cheng, Y. Pan, C. Li, H. Zhang, Preparation and characterization of silica aerogels from by-product silicon tetrachloride under ambient pressure drying, J. of Non-Cryst. Sol. 499 (2018) 387–393.
[44] S. Musić, N. Filipović-Vinceković, L. Sekovanić, Precipitation of amorphous sio2 particles and their properties, Br. J. of Chem. Eng. 28 (1) (2011) 89–94.
[45] Y.G. Kwon, S.E.Y. Choi, Ambient-dried silica aerogel doped with TiO2 powder for thermal insulation, J. of Mat. Sci. 35 (2000) 6075–6079.
[46] L. Zhu, Y. Wang, S. Cui, F. Yang, Z. Nie, Q. Li, Q. Wei, Preparation of Silica Aerogels by Ambient Pressure Drying without Causing Equipment Corrosion, Mol. 2018 (1935) 23.
[47] M.A. Worsley, T.T. Pham, A. Yan, S.J. Shin, J.R.I. Lee, M. Bagge-Hansen, W. Mickelson, A. Zettl, Synthesis and Characterization of Highly Crystalline Graphene Aerogels, ACS Nano 8 (10) (2014) 11013–11022.
[48] X. Xu, S. Fu, J. Guo, H. Li, Y.u. Huang, X. Duan, Elastic ceramic aerogels for thermal superinsulation under extreme conditions, Materials Today 42 (2021) 162–177.
[49] A.V. Fedyukhin, K.V. Strogonov, O.V. Soloveva, S.A. Solovev, I.G. Akhmetova, U. Berardi, M.D. Zaitsev, D.V. Grigorev, Aerogel Product Applications for High-Temperature Thermal Insulation, Energies 15 (2022) 7792.
[50] J. He, X. Li, D. Su, H. Ji, X.J. Wang, Ultra-low thermal conductivity and high strength of aerogels/fibrous ceramic composites, Journal of the European Ceramic Society 36 (6) (2016) 1487–1493.